F61: Nuclear Magnetic Resonance

Paris J. Huth & Q'inich Figueroa

May 2024

Abstract

In the experiment we study properties and usages of nuclear magnetic resonance (NMR). Firstly we measured the characteristic relaxation times T_1 and T_2 of two probes. The later of which was estimated with the Hahn echo and Carr-Purcell sequence. The results of which were then compared. Secondly NMR was used to identify substances using the characteristic chemical shift with TMS (Tetramethylsilane $\mathrm{Si}\,(\mathrm{CH_3})_4$) as reference substance. Lastly NRM was used for 1 dimensional and 2 dimensional imaging.

1 Theoretical and technical background

1.1 Basics of Nuclear Magnetic Resonance

Nuclear Magnetic Resonance techniques relay of the interaction between the magnetic dipole moment

$$\vec{\mu} = \hbar\gamma\vec{S} \tag{1}$$

of nuclei with non-zero spin S and an external magnetic field $\vec{B_0}$. Here γ represents the gyro-magnetic ratio of protons:

$$\gamma_{proton} = 2.6752 \cdot 10^8\,\mathrm{sec}^{-1}\mathrm{Tesla}^{-1}.$$

The resulting interaction energy, also called spin-lattice contribution, is defines as:

$$\Delta E = -\vec{\mu} \cdot \vec{B}_0. \tag{2}$$

This interaction yields two states for the orientation of the protons' magnetic dipole in the external magnetic field: μ_+ (parallel) and μ_- (anti-parallel). For a macroscopic sample of N protons, both numbers of occupied states N_+ and N_-, the sum of which comprises N, can be approximated by a Boltzmann distribution. Due to the parallel state being energetically favorable, one observes $N_+ > N_-$. The predominance of protons in the parallel state leads to a macroscopic magnetization. In our case, of a weak field ($\mu B \gg kT$), the ground state of the system can be approximated by:

$$\vec{M}_0 = \frac{N}{V}\frac{\hbar^2\gamma^2 I(I+1)}{3kT}\vec{B}_0 \propto \frac{\vec{B}_0}{T}, \tag{3}$$

i.e the law of Curie. Here $\hbar$ represents the normalized Plank's constant, k the Boltzmann constant, N stands for the number of particles of the sample, V its volume and T its temperature. I stands for the nuclear spin quantum number.

In general, the magnetization can have an arbitrary orientation related to the external magnetic field, however such a system will decay asymptotically into the ground state, since $\vec{M}_0$ minimizes the energy.

The interaction between the macroscopic magnetization and the external magnetic field result in a torque:

$$\vec{\tau} = \gamma \vec{M} \wedge \vec{B}_0. \tag{4}$$

If the magnetization is separated into parallel $\vec{M}_{\parallel}$ and perpendicular $\vec{M}_{\perp}$ components, relative to the external field, we see that only the later gives a non-trivial expression. Without any relaxation processes, the rate of change of $\vec{M}_{\perp}$ is given by:

$$\frac{d\vec{M}_{\perp}}{dt} = -\vec{M}_{\perp} \wedge \vec{B}_0. \tag{5}$$

The last equation describes the precession of $\vec{M}_{\perp}$ around $\vec{B}_0$. The angular frequency of this process is called the Larmor frequency:

$$\omega_L = \gamma B_0. \tag{6}$$

Generating a transverse or anti-parallel magnetization to $\vec{B}_0$ can be achieved by applying a high frequency pulse to the ground state magnetization $\vec{M}_0$.

For a static magnetic field $\vec{B}_0$ pointing in the z-direction, and a coil oriented along the x-axis, applying a sinusoidal voltage with a frequency ω_H, would generate a solenoid magnetic field $\vec{B}_1$ polarized along the x-direction. Under this conditions the torque acquires a second term:

$$\vec{\tau} = \vec{M}_0 \wedge \left(\vec{B}_0 + \vec{B}_1(t)\right) \tag{7}$$

which induces a second precession around the x-axis. For a pulse duration, which is short relative to the relaxation time, the magnitude of the magnetization is approximately constant. However, as explained above, the orientation of the vector changes throughout time, thus the point of the vector moves in a sphere with radius $|\vec{M}_0|$. In this case the vector coordinates can be fully described by a azimuthal angle φ, which is defined by the precession induced by $\vec{B}_0$, and by a polar angle θ which arises from the interaction with the solenoid field. Both angles are functions of time:

$$\varphi = \omega_L t \tag{8}$$

$$\theta = \gamma B_1 t. \tag{9}$$

A pulse which induces a polar angle $\theta = 90^\circ$ is called a 90° pulse. For such a pulse the ground state magnetization is transformed into transverse magnetization $\vec{M}_{\perp}$. Analogously a pulse which generates $\theta = 180$ is called a 180° pulse. Such a pulse transforms the ground state into an anti-parallel magnetization $\vec{M}_{\parallel} = -\vec{M}_0$.

1.2 NMR signal

1.2.1 Signal generation

In the set up used for this experiment, the high frequency pulses of fixed frequency $\omega_{HF} = 19.8$ MHz were generated in an electronic unit of the minispec p20. Said pulses induce a precession around the z-axis, that change the magnetic flux through the coil in time, resulting in a induction signal modulating by the Larmor frequency ω_L, which could be set up by hand. This signal is fed back to the p20 electronic unit, where both the high frequency and the induction signals are mixed into an output given by the multiplication of both inputs, i.g the sum of two cosine functions. One of the terms depends on the working frequency, which is given by the difference between ω_L and ω_{HF}, and is on the order of few hundred Hertz, while the second one in the range of 40MHz. The use of a low frequency bandpass filter allows to get rid of the later signal.

1.3 Relaxation Time

1.3.1 Bloch equations

For the description of the precession of $\vec{M}_\perp$ it is possible to define a rotating reference system (x', y', z). This reference frame is defined by 2 conditions: 1) the (x', y')-plane rotate in the static (x, y)-plane and 2) $\vec{M}_\perp$ points in the x'-direction, since we choose the rotating frame to rotate in the lab frame at the larmor frequency.

In this reference system the transverse and longitudinal magnetization are constant if no relaxations processes are present, otherwise both components are time dependent. Their time evolution is described by the Bloch equations:

$$\frac{d\vec{M}_\perp^{rot}}{dt} = -\frac{\vec{M}_\perp^{rot}}{T_2} \tag{10}$$

$$\frac{d\vec{M}_\parallel^{rot}}{dt} = -\frac{\vec{M}_\parallel^{rot} - \vec{M}^{rot}}{T_1}. \tag{11}$$

The constant T_2 in eq. 10 is the so called spin-spin relaxation time, whereas T_1 in eq. 11 is called the spin-lattice relaxation time. The ground state is equal in the rotating and the static reference frame.

In the presence of a relaxation processes, the time evolution of the magnetization in a laboratory $\vec{M}$ and in a rotating system $\vec{M}^{rot}$ are related : giving the following Bloch equations in laboratory system:

$$\frac{d\vec{M}_\perp(t)}{dt} = \gamma(\vec{B} \wedge \vec{M})_\perp - \frac{\vec{M}_\perp(t)}{T_2}, \tag{12}$$

$$\frac{d\vec{M}_\parallel(t)}{dt} = \gamma(\vec{B} \wedge \vec{M})_\parallel - \frac{\vec{M}_\parallel(t) - \vec{M}_0}{T_1}. \tag{13}$$

1.3.2 Spin-spin relaxation T_2

Due to the magnetic interactions between the sample's protons with themselves the system loose energy throughout time which results in a decay of $\vec{M}_\perp$ characterized by the relaxation time T_2. Said decay is described by the solution of eq. 12:

$$\vec{M}_\perp(t) = \vec{M}_\perp^0 e^{-\frac{t}{T_2}}. \tag{14}$$

This process is called spin-spin relaxation.

On top of this mechanism the slowly varying field inhomogeneities also contribute to the decay of the signal. This irregularities cause the protons at different positions to precess with different frequencies. Hence dephasing of the microscopic magnetizations takes place, which speeds the decay of the signal and thus results in a effective relaxation time T_2* smaller or equal to T_2. This doesn't allow a simple measurement of T_2. In order to measure the free induction decay's chareristic time, a 180° pulse is implemented, which corrects the dephasing of the magnetization.

In the following experiment two different methods were used to measure T_2: 1) spin-echo/ Hahn echo method and 2) Carr-Purcell sequence.

Spin-Echo: The spin echo method consist on a 90° pulse that creates a transverse magnetization followed by a 180° pulse at $t = \tau$ that reverts the dephasing. The 180° rotation along the x-axis caused by said pulse exchanges the position of protons that precess faster with the slow ones, but keeps the rotation direction invariant, all particles keep on rotating clockwise. Thus at $t = 2\tau$ the fast protons catch up with the slow ones generating a spin-echo. The process is illustrated in Fig. 1.

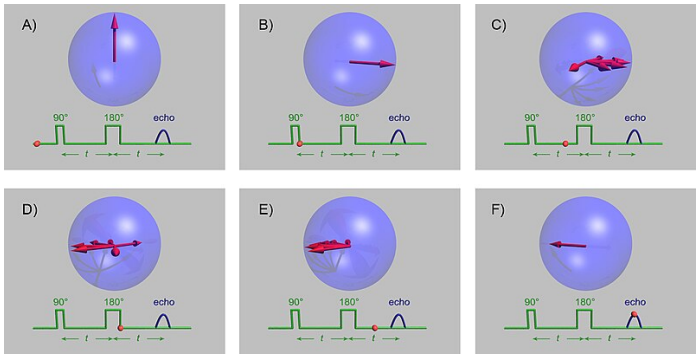

Figure 1: Spin-echo method. a) system in ground state, b) 90° pulse, c) dephasing, c) 180° pulse, d) rephasing, e) coherence state/ spin-echo [1]

[1] Nuclear magnetic resonance. (2024, May 16). Quelle: wikipedia.org

Due to Parseval's theorem it is possible to estimate the signal's strength by calculating the area under the spin-echo curvature in frequency space. The decay curve expressed in eq. 12 is measured by varying the parameter τ in the 90°-180° sequence.

The Hahn echo finds its limitations when measuring the decay curvature for large t. In such cases the time evolution, due to the field inhomogenieties, is faster than the time scale of the measurement τ, i.g the average Larmor frequencies in time intervals $0 < t < \tau$ and $\tau < t < 2\tau$ can be different. Hence, only partial coherence can be achieved, leading to reduced signals and a reduced value for T_2.

Carr-Pulcell sequence: The Carr-Purcell methods consists of a 90° pulse that creates a transverse magnetization followed by repeated 180° pulses at odd multiples of τ that induce phase coherence at even multiples of τ as shown in Fig 2. In this case τ is a small time interval. The sequence is repeated over a large interval of time yielding a value closer to the real value of the spin-spin relaxation time in comparison to the spin-echo method.

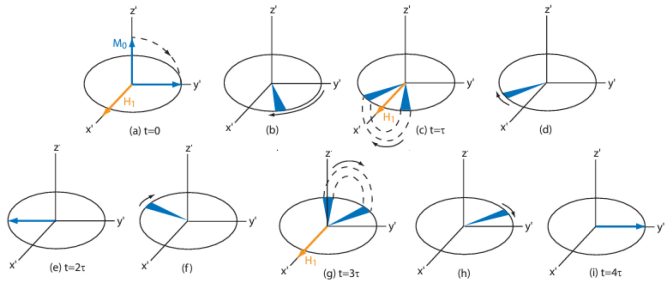

Figure 2: Carr-Purcell sequence. a) 90° pulse, b) dephasing of magnetization, c) 180° pulse at $t = \tau$, d) rephasing e) spin-echo/ coherence at $t = 2\tau$, f) dephasing, g) 180° pulse at $t = 3\tau$, h) rephasing, i) spin-echo at $t = 4\tau$. [2]

1.3.3 Spin-lattice relaxation T_1

An anti-parallel state will also decay by giving energy to its surroundings. This is the spin-lattice relaxation and it's described by the solution of eq. 13:

$$\vec{M}_{\parallel}(t) = \vec{M}_0 \left(1 - 2e^{t/T_1}\right). \tag{15}$$

After a 180° pulse a magnetization $\vec{M}_{\parallel}$ is generated, which is anti-parallel relative to the orientation of the field B_0. Since an anti-parallel state doesn't produce a signal, a 90° pulse at $t = \tau$ is used to transform the magnetization into a transverse one. The signal at $t = \tau$ is proportional to the initial longitudinal state. The decay curve of $\vec{M}_{\parallel}$ can be measured by varying the value of τ in the pulse sequence 180°-90°.

[2](2013, March 13). Physikalisches Praktikum im Bachelor-Studiengangander RWTH Aachen Versuch:Nuclear Magnetic Resonance(NMR) p. 16

1.4 Chemical shift

Protons that are bounded to molecules do not interact with the external magnetic field alone, but rather with a field $\vec{B}_{tot}$ modified by the magnetic shielding of the electron orbitals. Hence, according to equation 6, the Larmor frequency of the protons should be modified:

$$\omega_i = \omega_L \left(1 - \sigma_i\right). \tag{16}$$

Here ω_L is the free Larmor frequency, ω_i is the frequency modified by the chemical shift and σ_i stands for the shielding factor, which is characteristic for the molecule and each nucleus within the molecule.

In order to use this characteristic shielding factor to identify molecules a reference substance is added. This is done in order to achieve a set-up independent measurement which ensures the reproduction of such experiments. In order to do so the difference between the chemical shift of the reference substance and the chemical shifts of the unknown sample are measured rather than the chemical shift of the unknown molecule alone. For this experiment Tetra-Methyl-Silan (TMS) is used as reference substance. Under this condition the relative chemical shift δ_i is given by:

$$\delta_i = \sigma_i - \sigma_{TMS} = \frac{\omega_{TMS} - \omega_i}{\omega_L}. \tag{17}$$

Fig. 3 contains a chart with the measured relative chemical shift of different organic compound, the measurements are in units ppm (part per million).

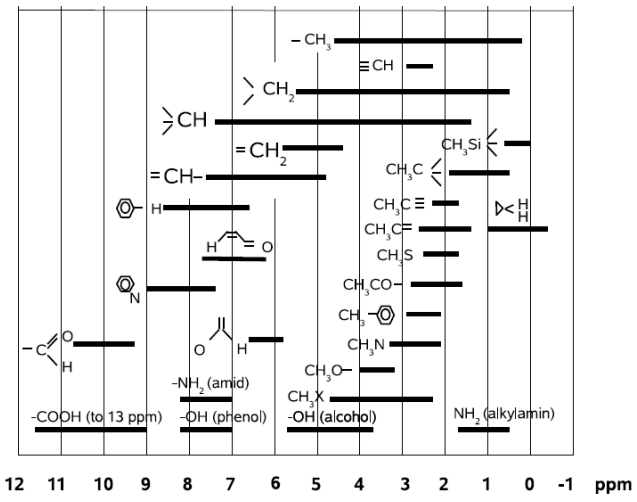

Figure 3: Chemical shift δ_i of different compounds relative to TMS [3]

[3] R. Schicker (2021, March 4). Nuclear Magnetic Resonance F61/F62 p. 19

1.5 Imaging with NMR

The imaging measurements in the experiment were made with the Bruker NMR analyzer mq7.5. In order to carry out measurements, which contain information on the position of the produced NMR signal, position dependent fields are implemented. These fields are superimposed to the static field $\vec{B}_0$ which defines the z-axis. In the used set up all gradients are chosen such that they point in z-direction and are linear functions of the corresponding coordinates:

$$\vec{B}^x = (0, 0, G^x \cdot x)^T$$
$$\vec{B}^y = (0, 0, G^y \cdot y)^T$$
$$\vec{B}^z = (0, 0, G^z \cdot z)^T$$

1.5.1 One dimensional imaging

Let's consider the 1 dimensional imaging in z-direction, where only the $\vec{B}^z$ is used.

Due to the field gradient the Larmor frequency becomes a linear function of position z:

$$\omega_L(z) = \gamma(B_0 + G^z \cdot z). \tag{18}$$

After taking the rotating frame into consideration, where $\vec{M}_\perp$ is given by eq. 12 and will be denoted as $\vec{M}_\perp^{rot}$, and the position dependent Larmor frequency in eq. 18 we can write the transverse magnetization as:

$$\vec{M}_\perp(z, t) = M_\perp^{rot}(z) e^{i\gamma(B_0 + G^z z)t}. \tag{19}$$

Using this expression one finds that the NMR signal is, apart from a phase factor, the Fourier transformation of the transverse magnetization $M_\perp^{rot}$:

$$S(t) \propto e^{i\Omega t} \int_V M_\perp^{rot}(z) e^{i\omega_z t} d\vec{x}. \tag{20}$$

Here it's worth noticing that we assumed $\vec{M}_\perp$ to be constant in time since the acquisition time is short wrt. T_2 ant the signal that we get is integrated over the whole slice. We the conclude that $M_\perp^{rot}(z)$ can be deduced from the measured NMR signal $S(t)$ by a 1 dimensional Fourier transformation signal. For the measurements there are two methods to generate the data points:

Frequency coding In this case the signal is measured as a function of time and we sample over $t_n = n\Delta t$ which gives a data set:

$$S_1 = S(\Delta t), \quad S_2 = S(2\Delta t), ..., S_N = S(N\Delta t)$$

Phase coding In this approach we use the fact, that during the readout the position information is related to the phase angle produced by the applied gradient:

$$\Delta\phi(z) = \phi(z) - \phi(0) = \gamma G^z z t = \omega_z t. \tag{21}$$

Thus the gradient G^z is applied during a time interval T_{Ph} before the read out, which induce a phase angle

$$\phi(z) = (\gamma G^z T_{Ph}) z = k_z z. \tag{22}$$

Here k_z is the position frequency. After this time the gradient is switched off. All the components of the magnetization precess with the original frequency but with different phase angles. To generated the data points the NMR signal is measured at a fixed time t_0 and sampled over different position frequencies $k_n = n\Delta k$ by varying the gradient strength in steps of ΔG^z. This results in the data set:

$$S_1 = S(\Delta k_z, t_0), \quad S_2 = S(2\Delta k_z, t_0), ..., S_N = S(N\Delta k_z, t_0).$$

1.5.2 Two dimensional imaging

For two dimensional imaging we use a two dimensional Fourier method. In this case the measurement method consist in first choosing a slice $z_1 < z < z_2$ which will be selectively excited by a high frequency pulse of duration t_p. At this point the different positions in the slice have different Larmor frequencies due to the slice selection gradient. To generate a phase coherent system, a second high frequency pulse with opposite polarization of the duration $t_p/2$ is used. Consequently we implement a combination of phase coding in x-direction and frequency coding in y-direction to generate a matrix of $N \times M$ data points $S(k_n, t_m)$. Finally the image can be derived by a two dimensional Fourier transformation.

2 Measurements Procedure

2.1 Relaxation time

In this part of the experiment we study the relaxation times T_1 and T_2 of two samples of Gadolinium mixed with different rations of water (Gd:water): Gd500 (1:5) and Gd600 (1:6). For that we first start by calibrating the magnet of the p20 unit by inserting the Gd600 sample and setting the 90° pulse for it to maximize the received signal. Analogously the 180° is set up for it to minimize the NMR signal, which ideally would be 0.

During the procedure of this experiment it was not possible for the 180° pulse to be set up to zero, however a minimum was found and the pulse was set for this later. This is a technical issue, which originated from the used experimental set-up itself. The machine used lacked of a fine tuner that would make the calibration more precise. After calibration the measurements are taken as previously described: For T_2 we use the Hahn echo method and Carr-Purcell metod, whereas for T_1 we implement a 180°-90° sequence. During the entirety of this measurement the working frequency was set to $\omega_w = (1 \pm 0.5)$ kHz.

2.2 Chemical shift

Next we use the NMR to identify 5 substances. For the identification of the probes we use TMS as a reference substance, hence we have two samples for each probes: one for the unknown substance alone and a second sample mixed with TMS.

The samples are inserted in the magnet of the p20 unit, then the probe are rapidly rotate using compressed air. This procedure was implemented to minimize the field inhomogeneities, hence minimizing the width of the signal in frequency space. Consequently we perform a spin-echo measurement. The signal is Fourier transformed and a Gaussian profile is fitted into the different peaks of the spectrum to measure the frequency of the maxima. These peaks correspond to the active groups of the molecule. The spectrum of the sample without TMS is compared to the one with TMS to identify the position of the reference substance's maximum. Finally the relative distance between the TMS-maximum and the active group's maxima is measured. In Fig. 3 the black lines besides the chemical formula of the organic compounds give the possible range for the relative chemical shift of said substance. So, we use the measured δ and search for the groups in Fig. 3 that matches it. Once the active compounds are known we search for the matching molecules in Fig. 4.

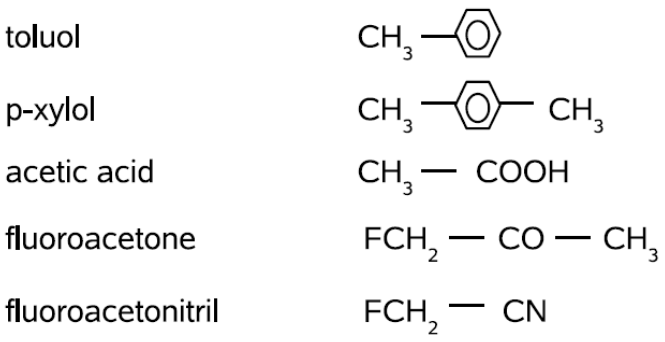

Figure 4: Five substances for identification [4]

2.3 Imaging

The last part of the experiment consist of 3 small tasks. All of them were performed using a Bruker minispec mq7.5 directly connected to a computer.

1 dimensional imaging In this part we introduce three different samples and study their 1 dimensional profiles.

[4] R. Schicker (2021, March 4). Nuclear Magnetic Resonance F61/F62 p. 20

Time evolution of system We prepare a test tube with 15 ml of sand. About 4 ml of oil are poured into the test tube. The prepared vial is quickly placed into the NMRI device. To study the time evolution of this test tube we take different 1 dimensional profiles throughout a time interval.

2 dimensional imaging We place different objects in the NMRI machine and take 2D profile of them.

3 Results

3.1 Relaxation time

The variation of parameter τ in the spin-echo and 180°-90° sequence allowed us to measure the time evolution of the transverse (Fig. 5a & Fig. 5b) and anti-parallel magnetization (Fig. 7a & Fig. 7b). A second measurement for the transverse component using the Carr-Purcell sequence delivered Fig. 6a & Fig. 6b.

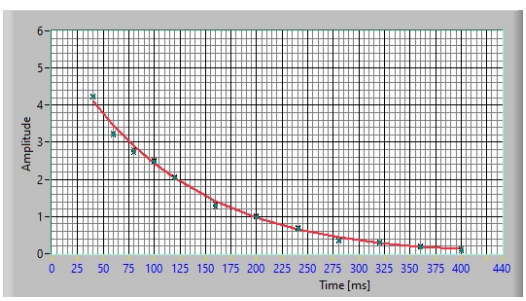

(a) GD500

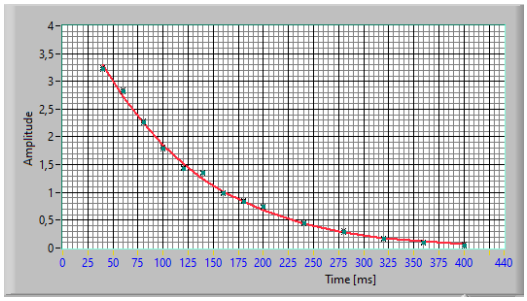

(b) GD600

Figure 5: Decay curve of $M_\perp$ measured with spin-echo methode

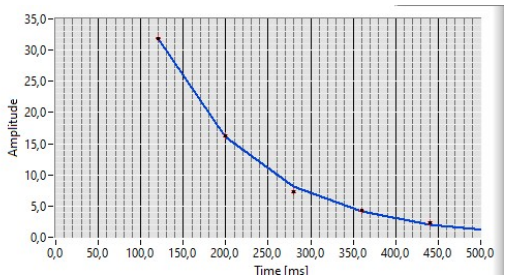

(a) GD500

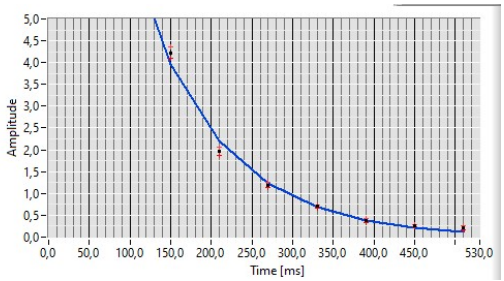

(b) GD600

Figure 6: Decay curve of $M_\perp$ measured with Carr-Purcell sequence

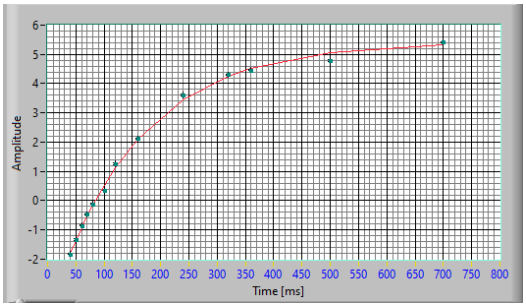

(a) GD500

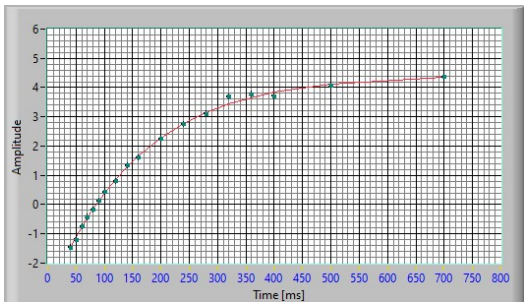

(b) GD600

Figure 7: Decay curve of $M_{\|}$ measured with 180°-90° sequence

A quick glance at the curves tells us that the time evolution of the components of the magnetization is described by decay curves, as we expected from the solutions of the bloch equations (eq.15 & eq. 14). By fitting these equation to our data, we were able to find the characteristic relaxation times T_1 and T_2. The results of the measurements are summarized in Tab. 1. Here the fourth column, deviation σ, represents the deviation from the methods used to measure T_2:

$$\sigma := \frac{|T_{2,sp.echo} - T_{2,CP}|}{\sqrt{\Delta T^2_{2,sp.echo} + \Delta T_{2,CP}}}.$$

Table 1: Relaxation times for Gd500 and Gd600

Probe	T_2 [ms] spin-echo	T_2 [ms] Carr-Purcell	deviation σ	spin-lattice T_1[ms]
Gd 500	110 ± 6	111,3 ± 1,5	0,5	159 ± 1,3
Gd 600	115,7 ± 1,2	116,9 ± 0,9	0,8	154,4 ± 1,2

Firstly, we observe that the spin-spin relaxation time of the probe with lower density, Gd600, is larger than that of Gd500, as expected. From our theory we know that T_2 is mainly determined by the interaction between the proton's spins. Hence the bigger the concentration, which translates to a larger amount of protons therefore of spins, the more possibilities there exist for a proton to dissipate its excitation energy resulting in a smaller spin-spin relaxation time.

Secondly we observe that $T_{1,Gd500} > T_{1,Gd600}$, which contradicts our expectations. Analogously to the case of T_2, a higher concentration also translates in a smaller spin-lattice relaxation time, since the excited state has a larger lattice in which it can dissipates its energy. This expectations also arise from the known paramagnetic characteristics of Gd, which enhance the local magnetic field. Hence the interaction with Gd-atoms result in a shorter relaxation.

From our experiment we can observe that the deviation between the results gained by the spin-echo and Carr-Purcell methods are not significant, however from our theory we know that this second method delivers more exact results. The Carr-Purcell sequence is also a faster measurement technique, since it can be completely automatized, thus reducing the susceptibility to human errors. Lastly we also observe a higher precision from this second method, it delivers a smaller uncertainty in all measurements. This last point is better observed by the measurements of Gd500 where the uncertainty of the spin-echo method is almost 4 times bigger than the one delivered by the Carr-Purcell sequence.

3.2 Chemical shift

The measured frequency spectra for the samples with and without the reference substance are to be seen in Fig.8 - Fig. 12.

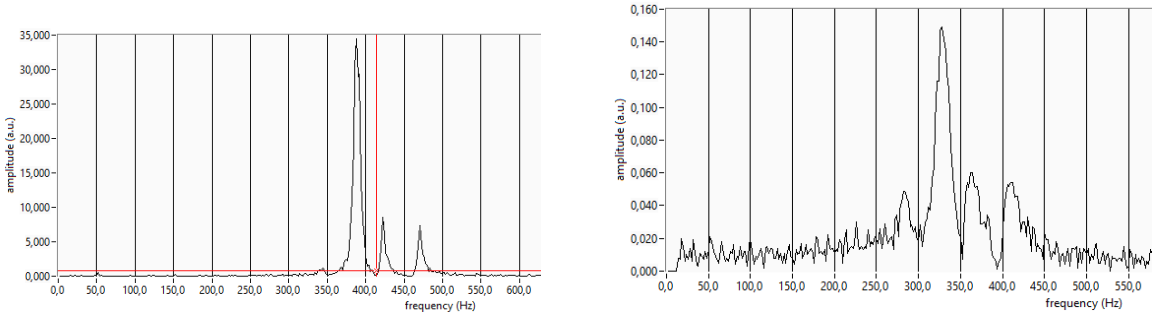

(a) Substance A (b) Substance A + TMS

Figure 8: Frequency spectrum of substance A

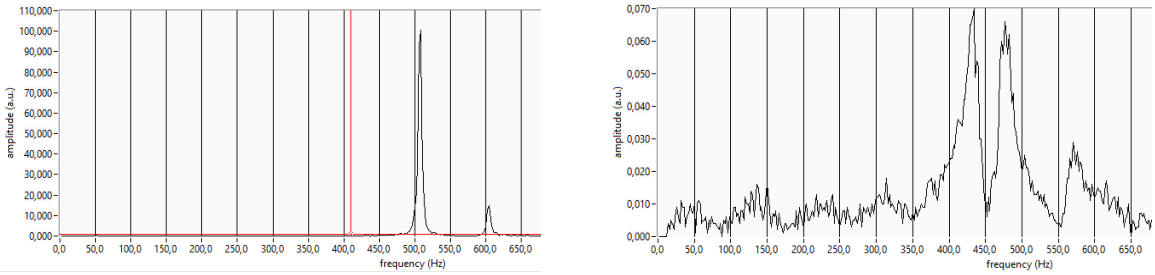

(a) Substance B (b) Substance B + TMS

Figure 9: Frequency spectrum of substance B

The measured relative distances between the maximum of TMS and the active groups of the probes are in Tab. 2 along with the names of the molecule matching the identified active groups.

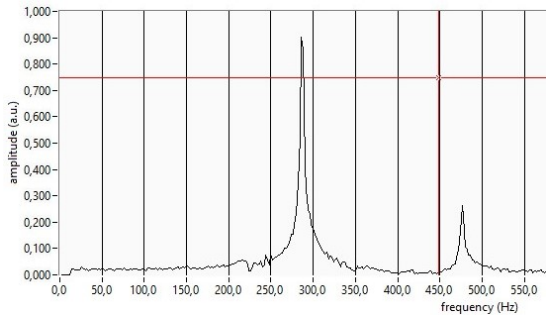

(a) Substance C

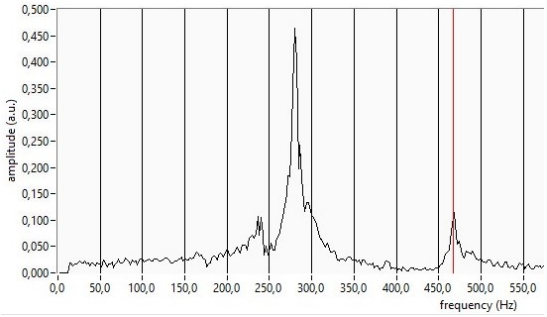

(b) Substance C + TMS

Figure 10: Frequency spectrum of substance C

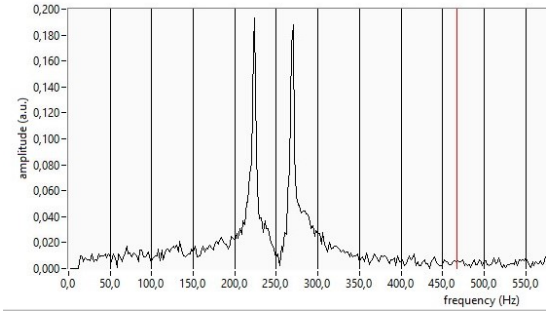

(a) Substance D

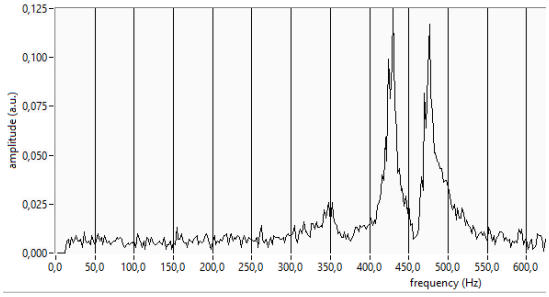

(b) Substance D + TMS

Figure 11: Frequency spectrum of substance D

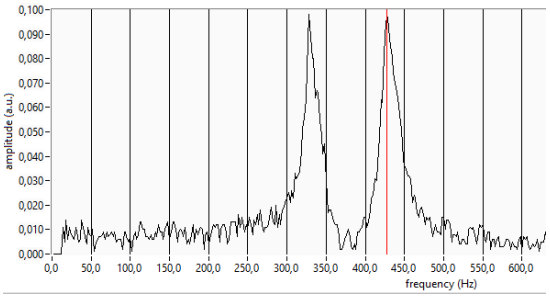

(a) Substance E

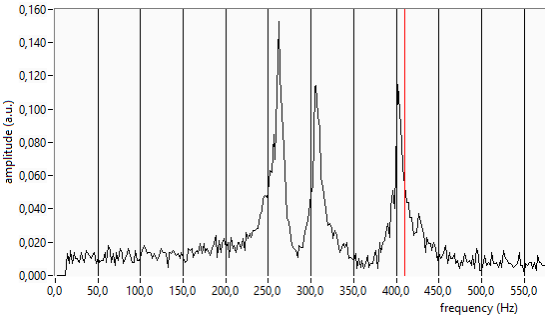

(b) Substance E + TMS

Figure 12: Frequency spectrum of substance E

Table 2: Measured relative chemical and identification of probes

Probe	Relative distance Δ [ppm]			**Substance**
	Δ_1	Δ_2	Δ_3	
A	2,3	4,1	6,8	fluroacetone
B	2,5	7,2	-	p-xylol
C	2,2	11,8	-	acetic acid
D	4,1	6,5	-	fluroacetonitril
E	2,3	7,1	-	toluol

In the given list of molecules,see Fig. 4, we notice that fluroacetone is the only molecule with three maxima in its spectrum, since given its chemical components with one maximum corresponding to CH_3 and two lines for the FH_2 group. This line splitting arise from the extra magnetic energy given to this component. Therefore to identify probe A there is no need to measure the relative distances Δ_i, instead a qualitative study of its spectrum (Fig. 8) is sufficient to identify it as fluroacetone. A study of the measured relative chemical shift of D shows that it contains the 2 lines from the FH_2 group, which leads us to identify it as fluroacetonitril. On the other hand, we can see in Tab. 2 that probes B and E have the same active groups, however we see a higher intensity in the peak corresponding to the active group CH_3 in the spectra of probe B (Fig. 9a) in comparison to that shown in E's spectra (Fig. 12a). With this observation we are able to identify substance B as p-xylol and E as toluol. Lastly we identify probe C as acetic acid due to the big chemical shift Δ_2, which is caused by the active group $COOH$.

3.3 Imaging

1 dimensional imaging The signal obtained by a vertical imaging of two probes containing the same oil, but which differ in vertical extend and positioning, show disparities (see Fig. 13). In the vial with less volume we see a constant signal, with some noise on top of it, meanwhile we observe a increase in the signal of the vial with higher volume of oil in range $x < -15$ mm and $x > 15$ mm. This change in the measured signal is an effect caused by the non-linearity of the field gradient. It is know that the applied magnetic field is not perfectly linear. In conclusion, the probes have to be set in a position $x \in [-15$ mm, 15 mm] in order to minimize the the effect of non-linearity of the field gradient.

Secondly, we insert a probe containing oil and a piece of Teflon. The measured vertical profile (see Fig. 14) shows a pattern of peaks and valleys, revealing the structure of the teflon piece. Since it does not emit an NMR signal, the pattern implies the piece consisting of stacked Teflon plates. The valleys correspond to the presence of said plates. In these areas the signal is not zero, since there still oil around the probe which does emit a NMR signal. On the other hand, the peaks represent the areas where the plates are bonded to one another, and due to the higher volume of oil present in such areas, the measured signal

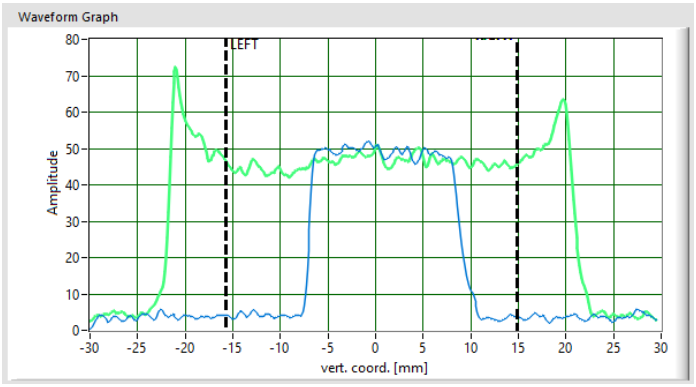

Figure 13: 1 dimensional NMRI of 2 oil samples. Blue line: short oil sample, green line: long oil sample

is stronger.

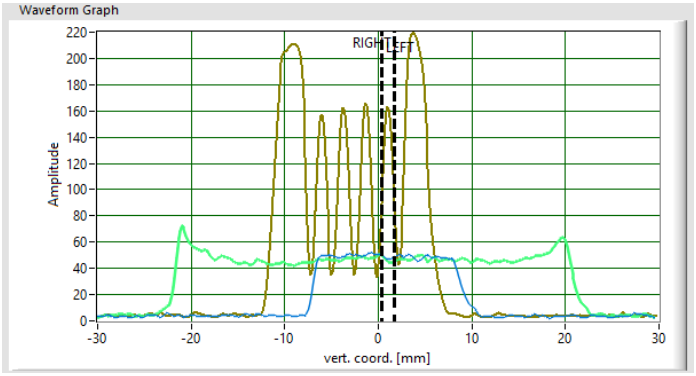

Figure 14: 1 dimensional NMRI of 2 oil samples & Teflon. Blue: short oil sample, green: long oil sample, brown: Teflon + oil

Time evolution of system The vertical profile was measured 96 times. The NRM signals Nr $1, 10, 30, 50, 96$ are plotted in Fig. 15. In this diagram we observe how the position curve develops a concavity. We remember that a diffusion process is described by the equation:

$$\frac{\partial u}{\partial t} = D\frac{\partial^2 u}{\partial x^2}. \tag{23}$$

Here D represents a constant which is always greater than zero, since for our material we observe an increase over time in the amplitude in the left side of Fig. 15. We further notice that since the concentration in the left part of the graph increases the time derivative

must be positive. So, for the differential equation to be satisfied the spacial curve should be convex, i.e the second derivative should also be positive, which clearly is not the case. Therefore we conclude that the oil pouring down through the sand is not a diffusion process. Instead, the found time evolution is proper of a percolation process, which describes the movement and filtering of fluids through porous materials.

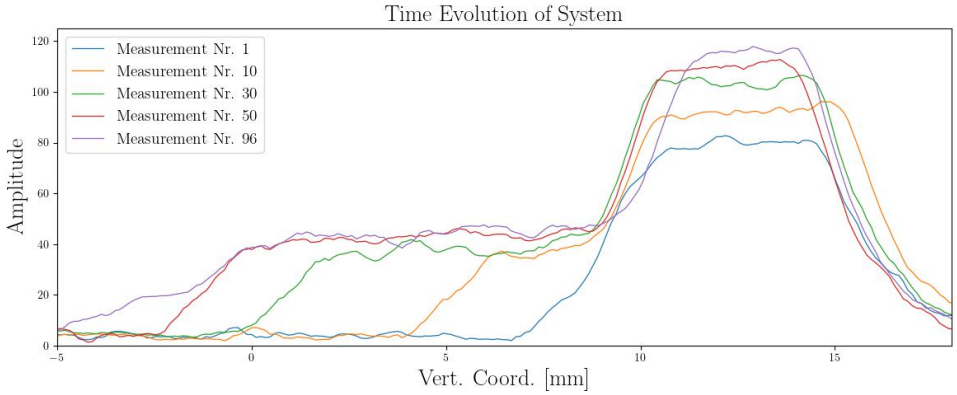

Figure 15: Time evolution of sand and oil probe.

2 dimensional imaging To get familiar with the measuring set up we started by taking horizontal and vertical scans of a vial filled with oil, see Fig. 16b & 16a. As expected, the measured signals are constant at the position of the probe tube, thus the images show the geometry of the used probe tube.

When studying a peanut, we first observed that due to the lack of water or fat in the nut's shell, it does not emit enough NMR. Hence, in the taken scan we can only see the inner structures of the peanut. In the scan Fig. 16c one can observe both nuts and the air gap between the two halves of the nut in the upper one. This gap can also be seen, with less resolution in the horizontal scan, see Fig. 16d.

Analogously if we place a pecan in the NMRI device, the shell does not emit enough NMR signal, thus we can only see the inner nut. See Fig. 16e.

Lastly we place a celery in the NMR machine, its horizontal profile can be seen in Fig. 16f. There we can see the C-shape of the branch. In the inner of the celery we also see slightly darker spots, which corresponds to holes filled with water. These spots are better visible in range $y \in [5, 20]$, however the resolution still not ideal.

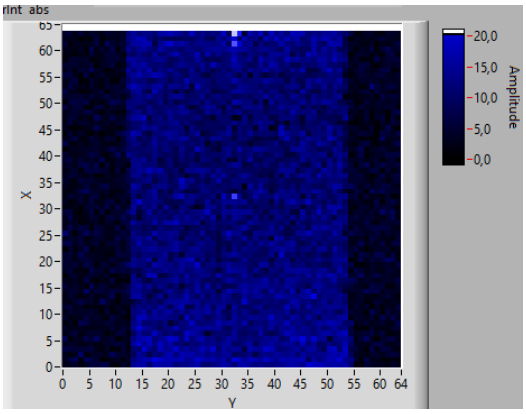

(a) vertical scan of oil

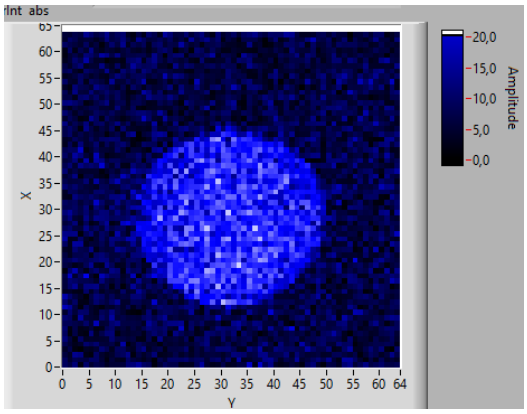

(b) horizontal scan of oil

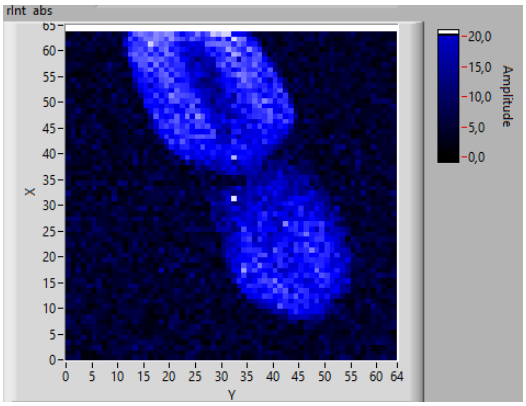

(c) vertical scan of peanut

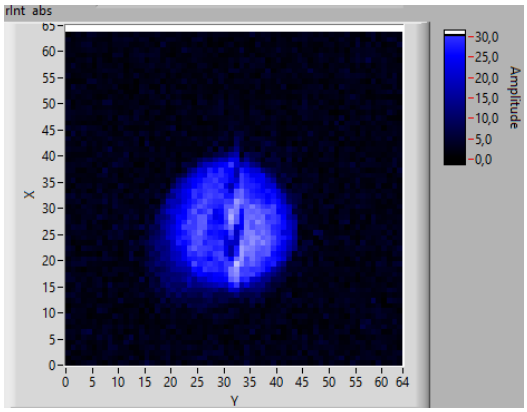

(d) horizontal scan of peanut

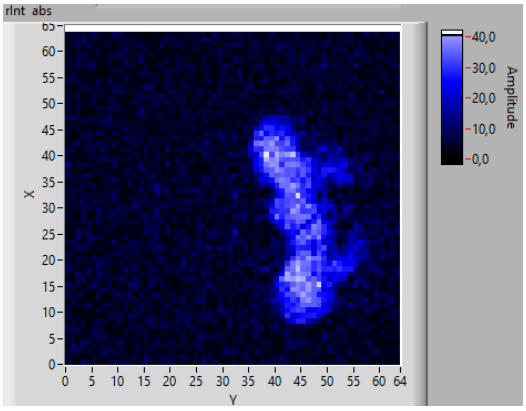

(e) horizontal scan of pecan

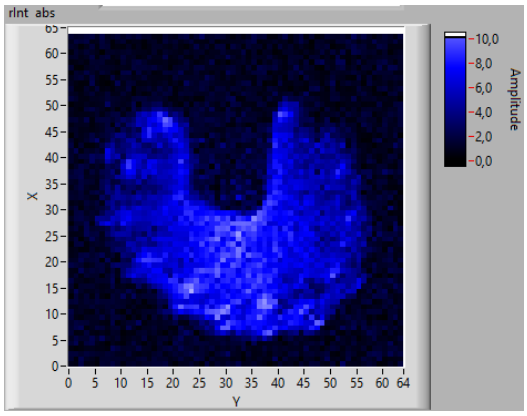

(f) horizontal scan of celery

Figure 16: 2D profiles of different objects

4 Critical Discussion

The goal of the experiment was to study and get familiar with the theory and implementations of nuclear magnetic resonance. For that we studied two methods to measure the spin-spin relaxation time and one to estimate the spin-lattice relaxation time.

We examined two samples, Gd500 (1 part Gd to 5 parts water) and Gd600 (1 part Gd to 6 parts water), for which we obtained T_1 times using 180°-90° sequences: $T_{1,500} = 159.01.3$ ms and $T_{1,600} = 154.41.2$ ms. These times decrease with an increase in gadolinium concentration, as expected, due to the increased potential to dissipate energy. However, the T_2 measurements did not follow this expected trend; both the spin-echo and Carr-Purcell values increased with a higher concentration. The spin-echo sequence yielded $T_{2,500} = 1106$ ms and $T_{2,600} = 115.71.2$ ms, and the Carr-Purcell sequence yielded $T_{2,500} = 111.31.5$ ms and $T_{2,600} = 116.90.9$ ms.

Repeated testing did not change the relationship of these values, leading us to the conclusion of a potential setup error, either in the NMR device itself or, more likely, the Gd500 or Gd600 samples. The deviation between the two methods of measurement does not seem significant, although we expect the results from the Carr-Purcell method to show a smaller deviation from the true value of T_2 for a given sample.

Later we identified 5 probes by measuring the relative chemical shift, where we used TMS as reference substance. We inserted each of the 5 probes, with and without the reference substance, and took measurements while rotating them with compressed air. The process of rotating proved to be somewhat finicky, which is why some of the spectra include more noise than the others. Nevertheless, we were able to identify all the probes, starting with substance A, which had to be fluroacetone because of its 3 distinct peaks, which no other probe could produce. Probe D showed the active group FH_2, which was already present in fluroacetone and thus had to be fluoroacetonitril. The spectrum of the probes B and E showed identical chemical shifts, although the intensity of the maxima varied. The maxima of probe B have show an increased intensity compared to probe E due to the presents of two CH_3 groups compared to the one group contained in probe E. Thus probe B being p-xylol and E being toluol. Lastly, probe C corresponded to acetic acid due to its big chemical shift by the active group $COOH$.

Next, we used NMR for imaging. In this last part we first got familiar with the operation by taking 1 dimensional scans. We examined different vials filled with oil and tested the extend of the viable measurement range. Values obtained outside the $x \in [-15mm, 15mm]$ range deviated in terms of intensity due to the non-linearity of the field gradient. This was obtained measuring two vials of oil of varying length. We also examined a vile containing a teflon probe. Since teflon does not produce a NMR signal, one could identify the structure of said probe by the lack of signal, caused by the displacement of oil.

Then we used 1 dimensional imaging to determine the nature of the time evolution of a system. A vial filled with sand was topped of with a few milliliters of oil and imaged over time. The measurements depict the movement and filtering of the fluid through the porous material, rather than a diffusion, since a concavity is clearly visible in the evolution of the

system.

Finally we use 2D imaging to map different objects and its structures. Starting off with the capturing of oil, both horizontally and vertically, to ensure expected behavior of system. After confirming, we continued on to imaging a peanut, trying to reveal both nuts inside its shell using a vertical scan, also showing the air gap within a single nut, in both the horizontal and vertical slice. It proved itself difficult setup the vertical and horizontal offset for imaging, and to choose the right slice thickness, to gain a satisfying result and signal strength, which is why we chose to continue with horizontal images. The scan of the pecan revealed the nut contained within its shell, and the celery showed its characteristic c-shape. One could also identify finer structures within the celery, due to its fitting setup and structure. The attempts at imaging a chili did not provide any viable results, due to yielding too weak of a signal, or low discernibility at higher slice thickness.